Neurobiology of Aging 36 (2015) 1792–1807

Contents lists available at ScienceDirect

Neurobiology of Aging

journal homepage: www.elsevier.com/locate/neuaging

Silibinin inhibits acetylcholinesterase activity and amyloid β peptide aggregation: a dual-target drug for the treatment of Alzheimer's disease

Songwei Duan [a,b], Xiaoyin Guan [a], Runxuan Lin [a], Xincheng Liu [a], Ying Yan [a], Ruibang Lin [a,b], Tianqi Zhang [a], Xueman Chen [a], Jiaqi Huang [a], Xicui Sun [c], Qingqing Li [a], Shaoliang Fang [d], Jun Xu [e], Zhibin Yao [a], Huaiyu Gu [a,*]

[a] Department of Anatomy, Zhongshan School of Medicine, Sun Yat-sen University, Guangzhou, China
[b] Guanghua School of Stomatology, Sun Yat-sen University, Guangzhou, Guangdong, China
[c] Guangzhou Brain and Psychiatric Hospital, Guangzhou, China
[d] Key Lab of High Performance Computing of Guangdong Province, Guangzhou, China
[e] Research Center for Drug Discovery and Institute of Human Virology, School of Pharmaceutical Sciences, Sun Yat-sen University, Guangzhou, China

ARTICLE INFO

Article history:
Received 29 April 2014
Received in revised form 3 February 2015
Accepted 4 February 2015
Available online 11 February 2015

Keywords:
Acetylcholinesterase
Alzheimer's disease
Amyloid β protein
APP/PS1 transgenic mice
MD simulation
Memory deficits
Silibinin

ABSTRACT

Alzheimer's disease (AD) is characterized by amyloid β (Aβ) peptide aggregation and cholinergic neurodegeneration. Therefore, in this paper, we examined silibinin, a flavonoid extracted from *Silybum marianum*, to determine its potential as a dual inhibitor of acetylcholinesterase (AChE) and Aβ peptide aggregation for AD treatment. To achieve this, we used molecular docking and molecular dynamics simulations to examine the affinity of silibinin with Aβ and AChE in silico. Next, we used circular dichroism and transmission electron microscopy to study the anti-Aβ aggregation capability of silibinin in vitro. Moreover, a Morris Water Maze test, enzyme-linked immunosorbent assay, immunohistochemistry, 5-bromo-2-deoxyuridine double labeling, and a gene gun experiment were performed on silibinin-treated APP/PS1 transgenic mice. In molecular dynamics simulations, silibinin interacted with Aβ and AChE to form different stable complexes. After the administration of silibinin, AChE activity and Aβ aggregations were down-regulated, and the quantity of AChE also decreased. In addition, silibinin-treated APP/PS1 transgenic mice had greater scores in the Morris Water Maze. Moreover, silibinin could increase the number of newly generated microglia, astrocytes, neurons, and neuronal precursor cells. Taken together, these data suggest that silibinin could act as a dual inhibitor of AChE and Aβ peptide aggregation, therefore suggesting a therapeutic strategy for AD treatment.

1. Introduction

Alzheimer's disease (AD) is a common and severe neurodegenerative disorder among elderly patients that is characterized by a cascade of pathologic changes. These changes include abnormal amyloid β (Aβ) peptide aggregation with the consequent formation of senile plaques in the cerebrocortical and limbic regions and a reduction in the levels of acetylcholine (ACh) (Isacson et al., 2002), together with progressive neuron loss (Gómez-Isla et al., 1997). Although considerable studies have been conducted on AD in previous years, the etiology of the disease remains unclear. Based on the cholinergic hypothesis of AD (Deutsch, 1971; Perry et al., 1999; Terry and Buccafusco, 2003), the current strategy of AD intervention is mainly to ameliorate the cognitive symptoms related to ACh depletion, thereby enhancing the central cholinergic neurotransmission by reversing acetylcholinesterase (AChE) inhibition. This hypothesis is based on several findings that cholinergic neurodegeneration can be a major pathologic feature in the brains of patients with AD, and experimental studies suggest ACh plays a vital role in learning and memory (Bloem et al., 2014).

Aβ aggregation is thought to be responsible for initiating the pathogenic cascade that results in neuronal loss and dementia (Estrada and Soto, 2007). Aβ aggregation has been shown to have crucial neurotoxic effects, which significantly supports the amyloid hypothesis (Haass and Selkoe, 2007; Skovronsky et al., 1998).

* Corresponding author at: Department of Anatomy, Zhongshan School of Medicine of Sun Yat-sen University, Guangzhou, Guangdong 510080, China. Tel.: (8620) 8733 2086; fax: (8620) 8733 2086.
E-mail address: gu_huaiyu@yahoo.com (H. Gu).

0197-4580/$ – see front matter © 2015 Elsevier Inc. All rights reserved.
http://dx.doi.org/10.1016/j.neurobiolaging.2015.02.002

Hence, the inhibition of Aβ aggregation and toxicity may carry therapeutic value by hindering the pathogenesis of AD (Hardy and Selkoe, 2002).

A previous study reports that cholinergic degeneration can accelerate Aβ plaque burden in vivo (Laursen et al., 2013). Additionally, it has been reported that AChE inhibitors can inhibit AChE-induced Aβ polymerization (Bartolini et al., 2003). One non-cholinergic role of AChE in the pathogenesis of AD is that AChE may play a substantial part in the development of the senile plaques by accelerating Aβ polymerization, which will induce greater neurotoxicity, depending on the amount of AChE bound to the complexes (Muñoz and Inestrosa, 1999). Dual inhibitors of both Aβ aggregation and AChE activity are considered to be potential therapeutic approaches that can slow or mitigate the progression of AD (Inestrosa et al., 2008; Yan and Feng, 2004).

Silibinin is a flavonoid extracted from the medicinal plant *Silybum marianum* (milk thistle) and traditionally has been used to treat liver diseases on account of its hepatoprotective properties (Křen and Walterova, 2005). In addition, silibinin can act as an antioxidant against oxidative stress-related neuropathy (Di Cesare Mannelli et al., 2012). Another study shows that silibinin can prevent Aβ-induced memory impairment and oxidative stress in male ICR mice (Lu et al., 2009; Yin et al., 2011). Furthermore, silibinin can attenuate streptozocin-induced memory impairment by reducing oxidative and nitrosative stress and synaptosomal calcium levels, thereby restoring the activity and mRNA expression of AChE (Tota et al., 2011). We assume that silibinin can inhibit Aβ aggregation and AChE activity simultaneously and impede the interaction between Aβ and AChE during AD pathogenesis. This effect may be attributed to the inhibitory effects of silibinin directly on the Aβ peptides, which differs from epigallocatechin gallate, another flavonoid that reduces Aβ aggregation through modulating amyloid precursor protein cleavage (Rezai-Zadeh et al., 2005).

In the present study, we attempt to explain the potential molecular mechanism of the inhibitory features by using a molecular dynamics simulation in silico, along with a series of assays that include circular dichroism (CD), transmission electron microscopy (TEM), and whole-cell patch-clamp in vitro and, ultimately studying the inhibition of Aβ aggregation and AChE activity in APP/PS1 transgenic (Tg) mice in vivo.

2. Methods

2.1. Animals

APPswe/PS1dE9 double Tg mice (strain type B6C3-Tg [APPswe, PSEN1dE9] 85Dbo/J; stock number 004462) were obtained from the Model Animal Research Center of Nanjing University (Nanjing, China). Age-matched wild-type (Wt) littermates were used as controls. The Sprague-Dawley rats were obtained from the Guangdong Medical Laboratory Animal Center (Foshan, China). All experimental procedures involving the animals were performed according to the regulations of the Institutional Animal Care and Use Committee of Sun Yat-sen University, Guangzhou, China. The mice and rats were housed at 25 °C and 60% relative humidity under a 12-hour light-dark cycle (light turned on at 7 AM) with ad libitum access to food and water. For this study, 50 Specific Pathogen Free (SPF) 8-month-old Wt and APP/PS1 double Tg mice were used (weight = 27.70 ± 3.47 g); 12 rats were assigned for these experiments. The number of female and male mice used for the study was equal to prevent sex differences from influencing the results.

Drosophila melanogaster stocks were reared on standard cornmeal agar medium supplemented with dry yeast at 25 °C and 60% relative humidity, and a previously developed method (Gu and O'Dowd, 2006, 2007) was used to examine the cholinergic miniature excitatory postsynaptic currents (mEPSCs) of the projection neurons (PNs) in the whole brain. *Drosophila melanogaster* matured into adults at approximately every 14 days. To record the *Drosophila* at accurate time points, all of the experiments were performed 2 days before eclosion on the Wt Canton-S female flies, which were identified by their red eyes and transparent wings in the puparium.

2.2. Drug administration

Because of its low solubility in water (80 μmol/L), silibinin was suspended in a 0.5% (w/v) carboxymethylcellulose sodium solution to enhance the solute concentration immediately before intraperitoneal injection with a constant volume of 10 mL/kg body weight this method ensured better drug absorption by the mice, compared with oral administration. Mice were administered silibinin (2, 20, and 200 $mg \cdot kg^{-1}$) or 0.5% carboxymethylcellulose sodium solution every day for 4 weeks. The animals were randomly divided into 5 groups of 10 mice each. The groups of Tg mice treated with 200, 20, and 2 $mg \cdot kg^{-1}$ of silibinin were named 200 mg, 20 mg, and 2 mg, respectively; the groups of Tg control and Wt control mice without silibinin treatment were named Tg Ctrl and Wt Ctrl, respectively. All of the mice were administered 50 mg/kg body weight 5-bromo-2-deoxyuridine (BrdU) each day for the first 5 days of the silibinin administration. For the following 23 days, the mice were administered only with silibinin. Each group contained 5 male and 5 female mice to control eventual sex differences from confounding the results.

In the pharmacokinetics study, silibinin and phosphate-buffered saline (PBS) were administered intravenously through the left jugular vein, while the right jugular vein was clipped to concentrate the drug. The groups were administered with 1 mL of PBS and 0.01% silibinin, and cerebrospinal fluid (CSF) samples were collected 2 minutes after the injections were named Ctrl (n = 6) and 2 minutes (n = 6), respectively.

2.3. Molecular docking and molecular dynamics simulations

All simulations were based on the solution structures of the Human Aβ1-42 (*Hu*Aβ42; PDB code 1IYT) (Crescenzi et al., 2002) and the *Torpedo californica* AChE (*Tc*AChE; PDB code 2 WFZ) (Sanson et al., 2009), which were obtained from the Protein Data Bank. We clearly elucidate the reason why we used 1IYT in silico simulations in our Supplementary data. The missing and truncated residues of the *Hu*Aβ42 and *Tc*AChE were properly repaired with the Biopolymer module of SYBYL 1.1 (Tripos Inc, St. Louis, MO, USA). Program Autodock 4.0 (Morris et al., 1998) was used to identify the docking positions of silibinin for *Hu*Aβ42, *Hu*Aβ40, and the catalytic active site (CAS) of *Tc*AChE with the Lamarckian genetic algorithm. The grid map with 80*80*80 points spaced equally at 0.375 Å was generated with an AutoGrid program (Redwood Shores, CA, USA) to calculate the binding energies between the ligand and the receptors. The docking parameters were set to the default values, except for the number of GA runs (200) and energy evaluations (25, 000, 000). All docked conformations were clustered under a tolerance of 2 Å for the root mean square deviation (RMSD) and ranked according to the docking energies at the end of each run.

The AMBER11 simulation suite (Case et al., 2010) was applied for molecular dynamic simulations and data analysis. The all-atom point-charge force field (AMBER ff03), which had a good balance between the helix and sheet, was used to represent the peptides (Duan et al., 2003). The water solvent was explicitly represented by the TIP3P model (Jorgensen et al., 1983). The parameters for silibinin were generated as follows: the electrostatic potential of silibinin was acquired at the HF/6-31G** level after a geometry optimization

using the Gaussian03 program (Kudin et al., 2004); the partial charges were derived by fitting the gas-phase electrostatic potential using the restrained electrostatic potential method (Bayly et al., 1993), and the other force parameters of the silibinin molecule were taken from the AMBER GAFF (Wang et al., 2004) parameter set; the missing interaction parameters in the ligand were generated using antechamber tools in AMBER11. The system was first minimized using the steepest descent algorithms for 2000 steps. Then, we performed 30-nanosecond molecular dynamics simulations for *Hu*Aβ42 and 5-nanosecond simulations for *Tc*AChE with a normal pressure and temperature ensemble. The pressure was coupled to 1 bar with an anisotropic coupling time of 1.0 ps, and the temperature was kept at 300 K during the simulation with a coupling time of 0.1 ps. The long-range electrostatic interaction was computed using the Particle-Mesh Ewald method (Darden et al., 1993). SHAKE (Ryckaert et al., 1977) was used to constrain all bonds connected to hydrogen atoms, which enabled a 2.0-fs step in the simulation. Cut-offs of 1.2 nm were used for *Hu*Aβ42 and *Tc*AChE. There were 2 additional sodium ions in the case of the negatively charged Aβ and 9 for AChE. The binding free energies ($\Delta G_{binding}$) were computed with the generalized molecular mechanics. The Born surface area (MM_GBSA) approach (Fogolari et al., 2003) at 300 K was built in the AMBER11 program. In total, 50 snapshots were taken from the last 2-nanosecond trajectory of *Hu*Aβ42 and *Tc*AChE with intervals of 40 ps. The vibrational entropy contributions were then calculated with NMODE analysis (Chong et al., 1999), and 50 snapshots were accepted for the NMODE analysis. The aforementioned computation was performed using 192 AMD Opteron (tm) Processor CPUs (2.1 GHz).

2.4. Whole-cell patch-clamp from the PN of Drosophila melanogaster

Silibinin, dimethyl sulfoxide (DMSO), tetrodotoxin (TTX), picrotoxin (PTX) and the chemical products used to prepare the external and internal solutions were all purchased from Sigma-Aldrich Inc. (Shanghai, China). The silibinin was prepared as stock solutions in DMSO and diluted in external solutions to the appropriate concentration (100 μM) with a final DMSO concentration of less than 0.1%, which had no significant effects on the mEPSCs of PNs. The delivery and changes to the solution were performed using a gravity perfusion system, and the effects of the drugs were observed 5 minutes after application of the drug.

All of the brains were obtained from flies 2 days before eclosion. The entire brain, including the optic lobes, was obtained and prepared for recordings in standard external solution containing (in mM) 101 NaCl, 1 $CaCl_2$, 4 $MgCl_2$, 3 KCl, 5 glucose, 1.25 NaH_2PO4, and 20.7 $NaHCO_{23}$, pH 7.2, 250 mOsm as previously described (Gu and O'Dowd, 2006, 2007). For the cholinergic mEPSCs recordings, TTX (1 μM) was added to the external solution to block voltage-gated sodium currents, and GABAergic synaptic currents were blocked by PTX (10 μM). Voltage-clamp recordings were performed using patch-clamp electrodes (10–13 MΩ) filled with an internal solution containing (in mM) 102 K-gluconate, 0.085 $CaCl_2$, 1.7 $MgCl_2$, 17 NaCl, 0.94 EGTA, and 8.5 HEPES, pH of 7.2, and 235 mOsm. All recordings were made at room temperature, and only a single PN was examined in each brain. Electrophysiological signals were acquired with an EPC10 amplifier (HEKA Elektronik, Lambrecht/Pfalz, Germany) filtered at 2 kHz using a built-in filter and digitized at 5 kHz. The mEPSCs were detected via the Mini Analysis software (Synaptosoft, Decatur, GA, USA). The events were accepted for analysis only if they were asymmetrical, with an increasing phase faster than 3 ms and a slower decaying phase. In addition, the threshold criterion for inclusion was 3 pA. The comparison of the frequency and amplitude of mEPSCs before and after the application of silibinin was performed with a paired *t* test. All of the data were compared with a paired *t* test.

The morphology of the recorded PNs was confirmed using post-hoc staining with biocytin (0.4%; Sigma-Aldrich Inc). In summary, after fixation for 3 hours on ice, the brains were rinsed with PBS (0.01 M, pH 7.4) containing 0.1% Triton X-100. After being blocked with 10% goat serum in PBS (0.01 M, pH 7.4) containing 0.1% Triton X-100, the brains were incubated in 1:10 mouse nc82 monoclonal antibody (The Developmental Studies Hybridoma Bank at the University of Iowa, Iowa City, IA, USA) and then incubated in 1:200 goat anti-mouse Alexa Fluor 488 overnight (A11001, Invitrogen, Grand Island, USA) and 1:200 streptavidin-CY3 (Molecular Devices, Sunnyvale, CA, USA). A Zeiss LSM 710 confocal microscope with a 40x water-immersion objective and z-stack was used to acquire the photos of dendritic arborization of the visual PNs. The 3D post-recording image processing was reconstructed using Imaris 6.4.2 software (Bitplane, Zurich, Switzerland).

2.5. AChE activity assays

AChE activity assays were carried out based on the colorimetric method (Ellman et al., 1961). AChE (E.C. 3.1.1.7, from electric eel), butyrylcholinesterase (BChE; E.C. 3.1.1.8, from equine serum), 5,50-dithiobis- (2-nitrobenzoic acid) (Ellman's reagent), butylthiocholine chloride, and acetylthiocholine chloride were purchased from Sigma-Aldrich Inc. The assay mixture containing enzyme, buffer, and inhibitor was incubated for 15 minutes before the substrate was added to initiate the reaction. Readings were taken at 10-second intervals for 2 minutes. Additionally, we used BChE as a Ctrl group to illustrate the specificity of silibinin to AChE. The BChE assay used the method described previously.

2.6. CD and TEM

Aβ1-42 (Sigma-Aldrich Inc.) was freshly dissolved in 0.01 M phosphate buffer (pH 7.4) at a concentration of 1 mg/mL. Then, 50 μM Aβ1-42 was incubated in the presence or absence of 50 μM silibinin for 3 days at 37 °C. CD spectra were recorded from 190 to 260 nm at the indicated time intervals; the secondary structures of treated and untreated Aβ1-42 samples were recorded at 25 °C with a Chirascan circular dichroism spectrometer (Applied PhotoPhysics, Surrey, UK) and repeated twice; and the data were converted to mean residue ellipticity as previously described (Sreerama and Woody, 2004). These Aβ1-42 structures were confirmed with TEM. An aliquot (5 μL) of each sample was spotted onto a glow-discharged, carbon-coated formvar copper grid and stained with 5 μL of 2% phosphotungstic acid (pH 7.0) for 1 minute; the samples were then air dried and observed under a transmission electron microscope (FEI Inc., Valley City, ND, USA). All images were captured at a voltage of 80 kV.

2.7. High-performance liquid chromatography (HPLC)

Silibinin was detected with the HPLC method using a ÄKTA Purifier 10 (GE Healthcare, Madison, WI, USA). This system is designed for fast protein liquid chromatography and is compatible for HPLC assay. It was equipped with 288 nm UV detector and 250×4.6 mm I.D. C_{18} column (GL Science Inc, Tokyo, Japan) in our tests. The mobile phase was methanol-water containing 0.6% glacial acetic acid (50:50, v/v). The flow rate was 1.0 mL/min and the monitoring wavelength was 288 nm. This system was controlled, and the data were collected by UNICORN Control system.

The CSF samples are collected from the Cisterna Magna of the rats (Liu and Duff, 2008). The capillary tubes (outer diameter 1.5 mm, inner diameter. 0.86 mm; Sutter Instrument, Novato, CA,

USA) were connected to 1-mL syringes by PE25 tubing (RWD Life-science, Guangdong, China). After making the sagittal incision on the neck, the subcutaneous tissues and muscles were bluntly dissected. We used a capillary tube to penetrate through the dura mater immediately after drying the dura mater with a cotton swab. The CSF was collected into the capillary tube with a syringe. Approximately 200 μL of CSF sample was collected from each rat. Samples contaminated with blood were abandoned. All CSF samples were frozen in −80 °C until they were used.

The CSF samples were thawed in room temperature and 500 μL of ice-cold methanol was added to precipitate the protein. After 30 minutes of precipitation in −20 °C, the samples were centrifuged at 6000 g for 10 minutes. The supernatant was then removed and dried under nitrogen. The samples were reconstituted in 200 μL of the mobile phase and filtrated by 0.45-μm membranes before injecting into the HPLC system. Besides, the standard solutions of silibinin (resolved in mobile phase) were prepared at low level (0.01%) and high level (0.1%). A total of 200 μL of each quality-controlled solution was also injected into the HPLC system.

2.8. Morris Water Maze

The Morris Water Maze (MWM; MT-200, Chengdu, China) was used to evaluate the spatial learning of APP/PS1 Tg mice after silibinin treatment. According to Charles V. Vorhees' procedure (Vorhees and Williams, 2006), the MWM test consists of a consecutive 5 days learning trial and a 1 day probe trial. Altogether, there were 4 learning trials per day, each from a different starting position, and 24 hours after the end of the learning trials, the probe trials were immediately carried out for 1 day. The timer was set to 60 seconds and automatically stopped once the mouse reached the platform within the 60 seconds and remained on the platform for 5 seconds. The time required to locate and get onto the platform was recorded as the escape latency. The mice were manually moved to the platform and allowed to stay on the platform for 20 seconds if they could not find the platform. Only mice swimming faster than 8 cm/s were recorded for the analysis, and the data from floating mice were discarded. After each trial, mice were dried off in their housing facilities next to an electric heater for 30 minutes. The trajectory and escape latency of the mice were recorded, and the average escape latency was analyzed each day. Then, the probe trial was performed 24 hours after the completion of the learning trial. The platform was removed, and the probe trial was set to 60 seconds. In our experiment, we recorded the platform-site crossovers, the path length of each group in each quadrant and the duration of each group in each quadrant in the probe trials for 60 seconds.

2.9. Tissue preparation

After the behavioral tests, all of the mice were sacrificed under deep anesthesia (pentobarbital sodium, 40 mg/kg). In each group, 6 mice were randomly chosen and used for the immunohistochemistry assay and enzyme-linked immunosorbent assay (ELISA); the other 4 mice were used for the synaptic morphological analysis after DiI-labeling with a Gene Gun, each analysis had the same amount of male and female mice. The mice were anesthetized, and venous blood was collected with serum separator tube, followed by transcardial perfusion with normal saline for 5 minutes, which included protease and phosphatase inhibitors. Then, the blood samples were allowed to precipitate for 2 hours at room temperature before being centrifuged for 15 minutes at 1000 g. The serum was removed, assayed immediately afterwards and stored at −80 °C. The brains of the 6 mice were removed and bisected sagittally. The right hemisphere was immediately frozen at −80 °C for biochemical analysis, and the left hemisphere was fixed and stored in 4% paraformaldehyde overnight, and dehydrated in 30% sucrose in 0.1 M phosphate buffer for 48 hours for immunohistochemical analysis, for which 40 μm thick free-floating coronal sections of fixed hemi-brains were collected using a freezing microtome (Leica, Wetzlar, Germany). We randomly collected 6 intact sections of each brain for the analysis. The other 4 mice were perfused with 2% paraformaldehyde for 24 hours; then the coronal sections (200 μm) were cut on a vibratome (Leica VT 1000 S), and one intact section was stored in 0.01 M PBS. The dentate gyrus and adjacent cortex −2.2 mm to −2.4 mm relative to the bregma were taken as the region of interest in both analyses.

2.10. Immunohistochemistry and immunofluorescence staining

Amyloid pathology was assessed using a primary antibody to Aβ1-42 (dilution, 1:2000; Invitrogen), labeled using a biotinylated secondary antibody (Invitrogen) for 1 hour at room temperature and visualized using DAB development. The surface area of the senile plaques were measured and compared as percentage of the dentate gyrus with Image-Pro Plus 6.0 (Media Cybernetics, Inc., Bethesda, Maryland, USA). BrdU was used to stain newly generated cells. The specimens were incubated with formamide, added to 2× saline sodium citrate (volume ratio was 1:1) at 65 °C for 2 hours and incubated in 2 M HCl at 30 °C for 30 minutes to unfold the DNA double helix structure. Next, the sections were washed with boric acid and PBS 3 times, and blocked with blocking buffer (5% bovine serum albumin and 0.03% Triton X-100 in PBS) for 30 minutes at 37 °C. The next day, the primary antibody rat anti-BrdU (1:400; Oxford Biotechnology, Lake Success, NY, USA) together with either mouse anti-neuronal nuclear antigen (NeuN, 1:400; Sigma-Aldrich Inc; to stain mature neurons), mouse anti-glial fibrillary acidic protein (GFAP, 1:10,000; Sigma-Aldrich Inc; to stain astrocytes), rabbit anti-Iba1 (ionized calcium binding adapter molecule, 1:500; Sigma-Aldrich Inc; to stain microglia) or goat anti- doublecortin (DCX, 1:40; Sigma-Aldrich Inc; to stain neonatal neurons) was added and incubated for 2 hours at 37 °C, then overnight at 4 °C. Afterward, a second corresponding fluorescent antibody was chosen to display the positive cells. To quantitate the labeled cells, the optical fractionator method using Stereo Investigator (MBF Bioscience, Williston, VT, USA) was used to count the number of all of the labeled cells. The cells double-labeled for BrdU+ and DCX+, BrdU+ and NeuN+, BrdU+ and Iba1+, and BrdU+ and GFAP+ were quantitated unilaterally in the subgranular zone of the hippocampus. The cell density was calculated from the sum of all cells counted, divided by the counting volume. We counted the number of labeled cells in 12 coronal sections per mouse brain that was stained and mounted on coded slides. The absolute numbers and ratios of double-labeled cells versus BrdU-positive cells were analyzed. Meanwhile, a Zeiss LSM 710 laser confocal scanning microscope (Carl Zeiss AG, Oberkochen, Germany) was used to record the immunohistochemical staining.

2.11. ELISA and AChE activity determination

In the ELISA, frozen brains were thawed and minced. Then, the cerebral tissues of the brain were weighed and homogenized in 50 mM Tris-HCl buffer, pH 8.0, containing a cocktail of protease inhibitors. The homogenates were centrifuged (100,000 × g, 1 hour, 4 °C), and the supernatants were stored at −70 °C for additional analysis of soluble Aβ, brain-derived neurotrophic factor (BDNF), and AChE. Then, we sonicated the pellet in 5 M guanidine Tris buffer; the samples were incubated for 30 minutes at room temperature, and then centrifuged (100,000 × g, 1 hour, 4 °C), and the supernatants were stored for analysis of insoluble Aβ.

The levels of Aβ1-40 and Aβ1-42 in mice brains were measured using ELISA. The concentrations of insoluble and soluble Aβ40 and Aβ42 were analyzed using Aβ ELISA kits (Invitrogen), following the protocol of the manufacturer. The levels of BDNF in the mouse brain and serum were measured with a Mouse BDNF ELISA Kit (CUSABIO, Wuhan, China) according to the manufacturer's protocol. And the AChE quantities were measured with a Mouse AChE ELISA Kit (CUSABIO) following the manufacturer's protocol. Finally, the AChE activities were determined using Ellman's method (Ellman et al., 1961). We used an Acetylcholinesterase Fluorescent Activity kit (Arbor Assays, Ann Arbor, MI, USA) to measure it according to the protocol of the manufacturer.

2.12. Diolistic labeling and morphological analysis

The gene gun bullets were prepared as described (Staffend and Meisel, 2011): to summarize, 4 mg of gold particles (1.6 μm diameter) were mixed with 2.5 mg DiI (Sigma-Aldrich Inc) and dissolved in 250 μL of methylene chloride. After drying, the coated particles were collected in 1.5 mL of water and placed into a sonicator for 5 minutes. The solution was vortexed for 15 seconds and immediately transferred to 1-mm diameter gene gun tubing (Bio-Rad, Hercules, CA, USA). The labeled sections were rinsed in 0.01 M PBS 3 times and resuspended in PBS at 4 °C overnight for the dye to diffuse through the neuronal membranes. The images of DiI-impregnated cells were taken using a Zeiss LSM 710 confocal microscope (Carl Zeiss). The neuron was scanned at 1-μm increments along the Z-axis and reconstructed using LAS AF software (Leica Microsystems, Buffalo Grove, IL, USA) to analyze the dendrite segments. The density of the dendritic spines was measured on 10–30 randomly chosen dendrites from 3 to 6 neurons, calculated by quantifying the number of spines per unit length of dendrite and normalized per 10 μm of dendrite length. 3D reconstructions of confocal images were performed with an Imaris 6.4.2 (Bitplane, Zurich, Switzerland).

2.13. Statistical analysis

The data represented as the mean ± SEM; $p < 0.05$ was considered to be significant. The statistical analysis of the MWM data was performed using a 2-way analysis of variance (ANOVA) for repeated measures, and a Bonferroni post-hoc test was used to perform the subsequent analysis if the data were significant in the previous ANOVA analysis. In the analyses of ELISA, immunohistochemistry assays, immunofluorescence assays and Diolistic labeling, a simple *t*-test was used to determine the difference between Wt Ctrl and Tg Ctrl, whereas the ANOVA was performed to assess the effect of silibinin within the Tg group. SPSS 13.0 software (SPSS Institute, Chicago, IL, USA) was used for all the statistical analyses.

3. Results

3.1. Silibinin binded with Aβ to form a stable complex in silico

The MD simulations were performed to investigate the stability of the silibinin-Aβ1-42 and silibinin-Aβ1-40 complexes according to the RMSD (Fig. 1A). The former complex remained constant at approximately 6 Å after 10 ns, and the variations were within 1 Å throughout the 3 repeated simulations. The latter complex was approximately 7 Å after 7 ns, and the variations were within 2 Å throughout the 3 repeated simulations.

The formation of the salt bridge between Asp23 and Lys28 in monomer folding plays a central role in the aggregation of Aβ (Lührs et al., 2005; Tarus et al., 2006). The distance between the Asp23 and Lys28 for Aβ1-42 and silibinin-Aβ1-42 was recorded every 1 ps during the computation, as shown in Fig. 1B. At approximately 24 ns, the distance between Asp23 and Lys28 sharply decreased in Aβ1-42 without silibinin binding (Fig. 1B), which suggested the formation of the Asp23-Lys28 salt bridge. When silibinin was bound to Aβ1-42, the distance between Asp23 and Lys28 held steady at approximately 15 nm for 30 ns. This result showed that the silibinin–Aβ1-42 complex has a lower formation probability for the Asp23–Lys28 salt bridge.

The conformations of Aβ1-42 and Aβ1-40 from 20 to 30 ns in the simulations were also analyzed and compared. The conformation of the silibinin-Aβ complex (Fig. 1C) was stable with a relatively constant proportion of α-helices and the presence of a turn structure. In contrast, the conformation of Aβ without silibinin binding (Fig. 1D) changed dramatically with a decreased α-helix proportion and the absence of a turn structure.

The helix structure correlates with the hydrophobicity of the residues, and the β-sheet structure is stabilized by hydrophobic interactions (Knecht et al., 2007). In fact, hydrophobic interactions were the most essential interactions between silibinin and Aβ. Thus, we calculated the solvent accessible surface area per residue to examine the extent of hydrophobic bonds in different regions of Aβ1-42 and Aβ1-40 with and without silibinin binding. The positive and negative values respectively revealed a decrease and increase in the hydrophobic character of the residues (Fig. 1E and F). This result suggested that silibinin weakened the hydrophobic interactions in the aggregation of Aβ1-42 and Aβ1-40.

The binding energy under each bond between Aβ and silibinin was calculated using the MM_GBSA method. The average decomposition of the total acquired binding energy revealed that the van der Waals and surface term (nonpolar solvation term) favored binding. The free binding energy of silibinin to Aβ1-42 was $\Delta G_{binding} = -11.7924$ kcal/mol (Table 1), which was close to the binding energy of the β-sheet breaker peptide LPFFD (Viet et al., 2011).

3.2. Silibinin binded to the active sites of AChE in silico

The MD simulations of AChE and its complex with silibinin were analyzed (Fig. 2A). To validate the stability of the simulation, the RMSD of the Cα of the complex versus the simulation time are shown in Fig. 2B. The values of the RMSD were approximately 1.5 Å, and the structure of AChE seemed to have been stabilized after 2 ns.

To investigate the interacting residues between AChE and silibinin, structural analyses were implemented to detect the hydrogen-bonding residues. AChE possesses 2 active sites that determine its catalytic activity; the CAS of AChE is located at the base of its long and narrow gorge and at the rim of the CAS is the peripheral anionic site (PAS) (Bourne et al., 2003). The 5 residues, Glu199, His440, Tyr121, Glu278, and Gly118, which are in both the CAS and PAS of AChE, formed hydrogen bonds with silibinin. The time dependence of the distances for these hydrogen bonds is shown in Fig. 2C. Three strong hydrogen-bonding residues, Glu199, His440, and Tyr121, with an average of 2 Å between silibinin and AChE, affected the binding affinity of the complex. A hydrogen bond interaction is thought to form if the distance between the hydrogen donor and acceptor is less than 3.5 Å (Steiner and Koellner, 2001).

Several studies have shown that π–π and π–H interactions play an important role in the stability of the protein structures, and the interactions are considered to be significant contributors to protein–ligand interfaces (Crowley and Golovin, 2005; Wintjens et al., 2000). The π-π interaction between silibinin and Tyr121, and π-H interactions between silibinin, Tyr67, and Tyr331 were observed in the silibinin–AChE system (Fig. 2D).

The binding energy under each binding mode of AChE and silibinin also was calculated using the MM_GBSA method. The binding

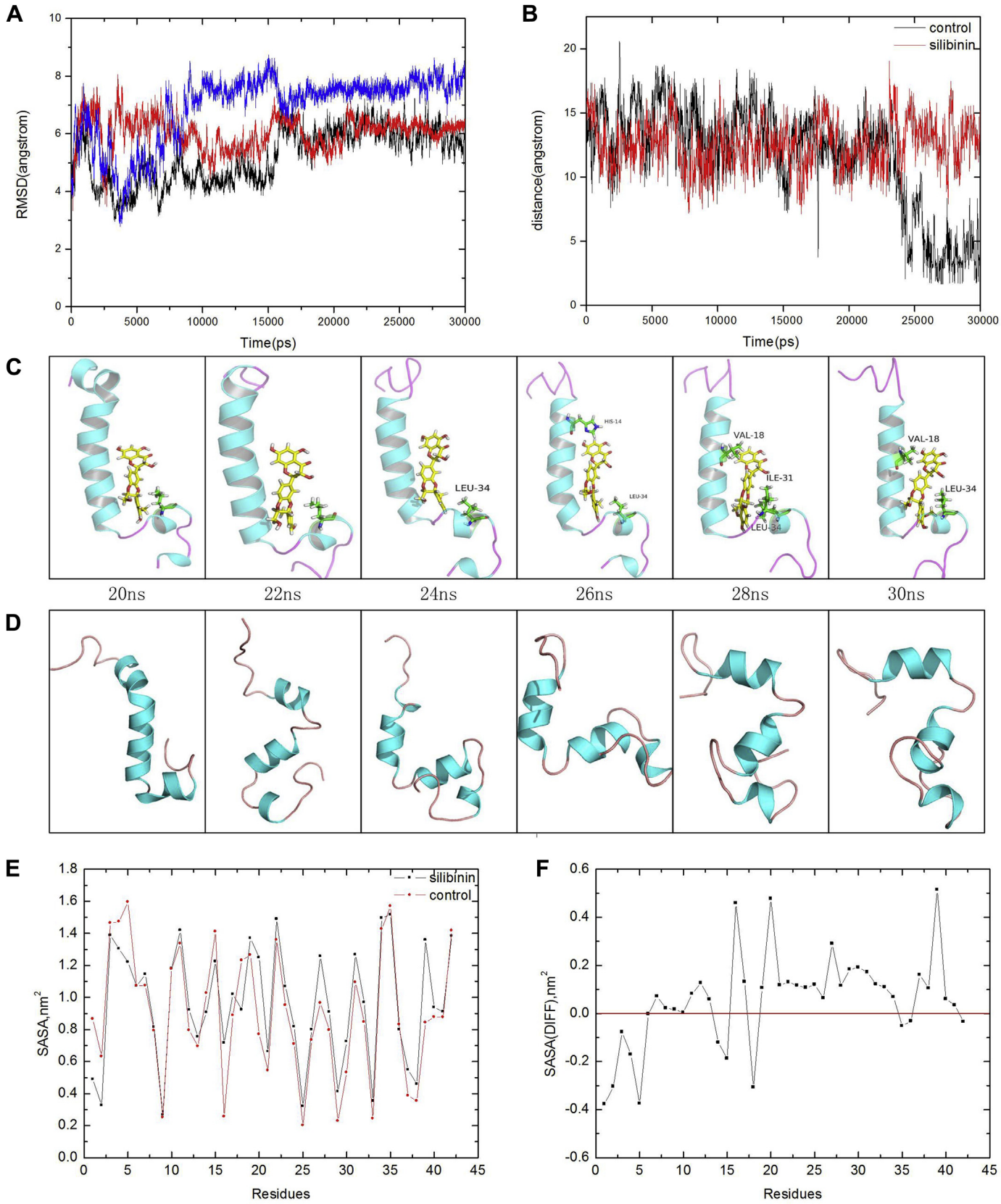

Fig. 1. Silibinin binds to Aβ to form a stable complex in silico. (A) The RMSD of the Aβ-silibinin complex. The root mean square distance of Aβ1-42 remains steady at approximately 6 Å in 3 repeated simulations, indicating that the complex is relatively stable. The red, blue, and black are 3 repeating trajectories for the MD simulations. (B) The distance between Asp23 and Lys28 of Aβ1-42. The distance between Asp23 and Lys28 remains constant at approximately 15 nm when silibinin is bound to Aβ1-42 (red), which suggests the absence of the Asp23–Lys28 salt bridge. The distance between Asp23 and Lys28 shows a sharp decrease in Aβ1-42 without silibinin binding (black), which suggests the formation of the Asp23–Lys28 salt bridge. (C) and (D) The conformation of Aβ1-42 during the MD simulation in the presence (C) and absence (D) of silibinin. The conformation of Aβ1-42 is stable